In vitro phosphorylation assays

For *in vitro* phosphorylation assays, Cos cells were transiently transfected with expression vectors encoding Flag-tagged HDACs or a Flag-tagged derivative of activated CaMKIV. Cells were collected in PBS containing 0.5% Triton X-100, 1 mM EDTA, 1 mM sodium pyrophosphate, 2 mM sodium fluoride, 10 mM β-glycerol phosphate, 1 mM sodium molybdate, 1 mM sodium orthovanadate, 1 mM PMSF and a protease inhibitor cocktail (Complete; Roche Molecular Biochemicals). Cells were sonicated briefly and cellular debris was removed by centrifugation. Flag-tagged proteins were immunoprecipitated using anti-Flag affinity resin (Sigma). Immunoprecipitates were washed two times in lysis buffer followed by three additional washes in a solution of 25 mM HEPES pH 7.6 and 10 mM $MgCl_2$. Where indicated, CaMKIV-bound beads were mixed with those bound to HDAC immediately before the addition of reaction buffer (40 μl) consisting of 25 mM HEPES pH 7.6, 10 mM $MgCl_2$, 2 mM $CaCl_2$, 20 μg ml^{-1} calmodulin, 12.5 μM ATP and [γ-^{32}P]ATP (10 μCi; 4,500 Ci $mmol^{-1}$). Reaction mixtures were incubated at 25 °C for 20 min. Reactions were terminated by addition of SDS–PAGE loading buffer followed by boiling. Immunoprecipitated proteins were resolved by SDS–PAGE, transferred to PVDF membranes and visualized by autoradiography followed by immunoblotting with anti-Flag antibodies.

Received 31 July; accepted 29 August 2000.

1. Molkentin, J. D., Black, B. L., Martin, J. F. & Olson, E. N. Cooperative activation of muscle gene expression by MEF2 and myogenic bHLH proteins. *Cell* **83,** 1125–1136 (1995).
2. Sparrow, D. B. *et al.* MEF-2 function is modified by a novel co-repressor, MITR. *EMBO J.* **18,** 5085–5098 (1999).
3. Miska, E. A. *et al.* HDAC4 deacetylase associates with and represses the MEF2 transcription factor. *EMBO J.* **18,** 5099–5107 (1999).
4. Lu, J., McKinsey, T. A., Nicol, R. L. & Olson, E. N. Signal-dependent activation of the MEF2 transcription factor by dissociation from histone deacetylases. *Proc Natl Acad Sci. USA* **97,** 4070–4075 (2000).
5. Lu, J., McKinsey, T. A., Zhang, C. L. & Olson, E. N. Regulation of skeletal myogenesis by association of MEF2 with class II histone deacetylases. *Mol. Cell* **6,** 233–244 (2000).
6. Kuo, M. H. & Allis, C. D. Roles of histone acetyltransferases and deacetylases in gene regulation. *BioEssays* **20,** 615–626 (1998).
7. Han, J., Jiang, Y., Li, Z., Kravchenko, V. V. & Ulevitch, R. J. Activation of the transcription factor MEF2C by the MAP kinase p38 in inflammation. *Nature* **386,** 296–299 (1997).
8. Kato, Y. *et al.* BMK1/ERK5 regulates serum-induced early gene expression through transcription factor MEF2C. *EMBO J.* **16,** 7054–7066 (1997).
9. Mao, Z. & Wiedmann, M. Calcineurin enhances MEF2 DNA binding activity in calcium-dependent survival of cerebellar granule neurons. *J. Biol. Chem.* **274,** 31102–31107 (1999).
10. Wu, H. *et al.* MEF2 responds to multiple calcium-regulated signals in the control of skeletal muscle fiber type. *EMBO J.* **19,** 1–11 (2000).
11. Nishi, K. *et al.* Leptomycin B targets a regulatory cascade of crm1, a fission yeast nuclear protein, involved in control of higher order chromosome structure and gene expression. *J. Biol. Chem.* **269,** 6320–6324 (1994).
12. Fukuda, M. *et al.* CRM1 is responsible for intracellular transport mediated by the nuclear export signal. *Nature* **390,** 308–311 (1997).
13. Gorner, W. *et al.* Nuclear localization of the C2H2 zinc finger protein Msn2p is regulated by stress and protein kinase A activity. *Genes Dev.* **12,** 586–597 (1998).
14. Beals, C. R., Sheridan, C. M., Turck, C. W., Gardner, P. & Crabtree, G. R. Nuclear export of NF-ATc enhanced by glycogen synthase kinase-3. *Science* **275,** 1930–1934 (1997).
15. Brunet, A. *et al.* Akt promotes cell survival by phosphorylating and inhibiting a Forkhead transcription factor. *Cell* **96,** 857–868 (1999).
16. Pinna, L. A. & Ruzzene, M. How do protein kinases recognize their substrates? *Biochem. Biophys. Acta.* **1314,** 191–225 (1996).
17. Grozinger, C. M. & Schreiber, S. L. Regulation of histone deacetylase 4 and 5 and transcriptional activity by 14-3-3-dependent cellular localization. *Proc. Natl Acad. Sci. USA* **97,** 7835–7840 (2000).
18. Sartorelli, V., Huang, J., Hamamori, Y. & Kedes, L. Molecular mechanisms of myogenic coactivation by p300: direct interaction with the activation domain of MyoD and with the MADS box of MEF2C. *Mol. Cell. Biol.* **17,** 1010–1026 (1997).
19. Mayford, M. *et al.* Control of memory formation through regulated expression of a CaMKII transgene. *Science* **274,** 1678–1683 (1996).
20. Passier, R. *et al.* CaM kinase signaling induces cardiac hypertrophy and activates the MEF2 transcription factor in vivo. *J. Clin. Invest.* **105,** 1395–1406 (2000).
21. Black, B. L. & Olson, E. N. Transcriptional control of muscle development by myocyte enhancer factor-2 (MEF2) proteins.. *Annu. Rev. Cell Dev. Biol.* **14,** 167–196 (1998).
22. Grozinger, C. M., Hassig, C. A. & Schreiber, S. L. Three proteins define a class of human histone deacetylases related to yeast Hda1p. *Proc. Natl. Acad. Sci.* **96,** 4868–4873 (1999).
23. Haribabu, B. *et al.* Human calcium-calmodulin dependent protein kinase I: cDNA cloning, domain structure and activation by phosphorylation at threonine-177 by calcium-calmodulin dependent protein kinase I kinase. *EMBO J.* **14,** 3679–3686 (1995).
24. Chatila, T., Anderson, K. A., Ho, N. & Means, A. R. A unique phosphorylation-dependent mechanism for the activation of Ca2+/calmodulin-dependent protein kinase type IV/GR. *J. Biol. Chem.* **271,** 21542–21548 (1996).
25. O'Keefe, S. J., Tamura, J., Kincaid, R. L., Tocci, M. J. & O'Neill, E. A. FK-506- and CsA-sensitive activation of the interleukin-2 promoter by calcineurin. *Nature* **357,** 692–694 (1992).
26. Jiang, Y. *et al.* Characterization of the structure and function of a new mitogen-activated protein kinase (p38beta). *J. Biol. Chem.* **271,** 17920–17926 (1996).
27. Rybkin, I. I., Cross, M. E., McReynolds, E. M., Lin, R. Z. & Ballou, L. M. alpha(1A) adrenergic receptor induces eukaryotic initiation factor 4E-binding protein 1 phosphorylation via a Ca(2+)-dependent pathway independent of phosphatidylinositol 3-kinase/Akt. *J. Biol. Chem.* **275,** 5460–5465 (2000).
28. English, J. M. *et al.* Contribution of the ERK5/MEK5 pathway to Ras/Raf signaling and growth control. *J. Biol. Chem.* **274,** 31588–31592 (1999).
29. Stambolic, V. & Woodgett, J. R. Mitogen inactivation of glycogen synthase kinase-3 beta in intact cells via serine 9 phosphorylation. *Biochem. J.* **303,** 701–704 (1994).
30. Mellon, P. L., Clegg, C. H., Correll, L. A. & McKnight, G. S. Regulation of transcription by cyclic AMP-dependent protein kinase. *Proc. Natl Acad. Sci. USA* **86,** 4887–4891 (1989).

Acknowledgements

We thank M. Cobb, J. Han, R. Lin, G.S. McKnight, A. Means, S. O'Keefe, S. Schreiber, T. Chatila and J. Woodgett for expression plasmids; R. Prives for anti-MEF2 antisera; and M. Yoshida for leptomycin B. We are grateful to A. Tizenor for graphics, and J. Page and W. Simpson for editorial assistance. E.N.O. was supported by grants from NIH, the Robert A. Welch Foundation, the D. W. Reynolds Foundation and Myogen, Inc. T.A.M. is a Pfizer fellow of The Life Sciences Research Foundation.

Correspondence and requests for materials should be addressed to E.N.O. (e-mail: eolson@hamon.swmed.edu).

Structural basis for signal transduction by the Toll/interleukin-1 receptor domains

Yingwu Xu*, Xiao Tao*, Baohe Shen*, Tiffany Horng†, Ruslan Medzhitov†, James L. Manley* & Liang Tong*

** Department of Biological Sciences, Columbia University, New York, New York 10027, USA*
† Section of Immunobiology, Yale University School of Medicine, New Haven, Connecticut 06520, USA

Toll-like receptors (TLRs) and the interleukin-1 receptor superfamily (IL-1Rs) are integral to both innate and adaptive immunity for host defence[1–3]. These receptors share a conserved cytoplasmic domain[4,5], known as the TIR domain. A single-point mutation in the TIR domain of murine TLR4 (Pro712His, the Lps^d mutation) abolishes the host immune response to lipopolysaccharide (LPS)[6], and mutation of the equivalent residue in TLR2, Pro681His, disrupts signal transduction in response to stimulation by yeast and Gram-positive bacteria[7]. Here we report the crystal structures of the TIR domains of human TLR1 and TLR2 and of the Pro681His mutant of TLR2. The structures have a large conserved surface patch that also contains the site of the Lps^d mutation. Mutagenesis and functional studies confirm that residues in this surface patch are crucial for receptor signalling. The Lps^d mutation does not disturb the structure of the TIR domain itself. Instead, structural and functional studies indicate that the conserved surface patch may mediate interactions with the downstream MyD88 adapter molecule[7–11], and that the Lps^d mutation may abolish receptor signalling by disrupting this recruitment.

A principal function of TIR domains is thought to be to mediate homotypic protein–protein interactions in the signal transduction process[2]. To elucidate the molecular basis of TIR domain signalling, we have determined the crystal structures of the TIR domains of human TLR1 and TLR2 (Table 1). The structures contain a central five-stranded parallel β-sheet (βA–βE) that is surrounded by a total of five helices (αA–αE) on both sides (Fig. 1a). To facilitate sequence and structure comparisons of this large family of protein domains, we use a residue numbering system based on the secondary structure elements observed in the current structures, similar to that adopted for *Src* homology (SH)-2 domains[12]. In the numbering system, a residue in a β-strand or α-helix is numbered according to its position in that strand or helix. The loops are named by the letters of the secondary structure elements that they connect. For example, the BB loop connects strand βB and helix αB. A residue in a loop is numbered according to its position in that loop, or

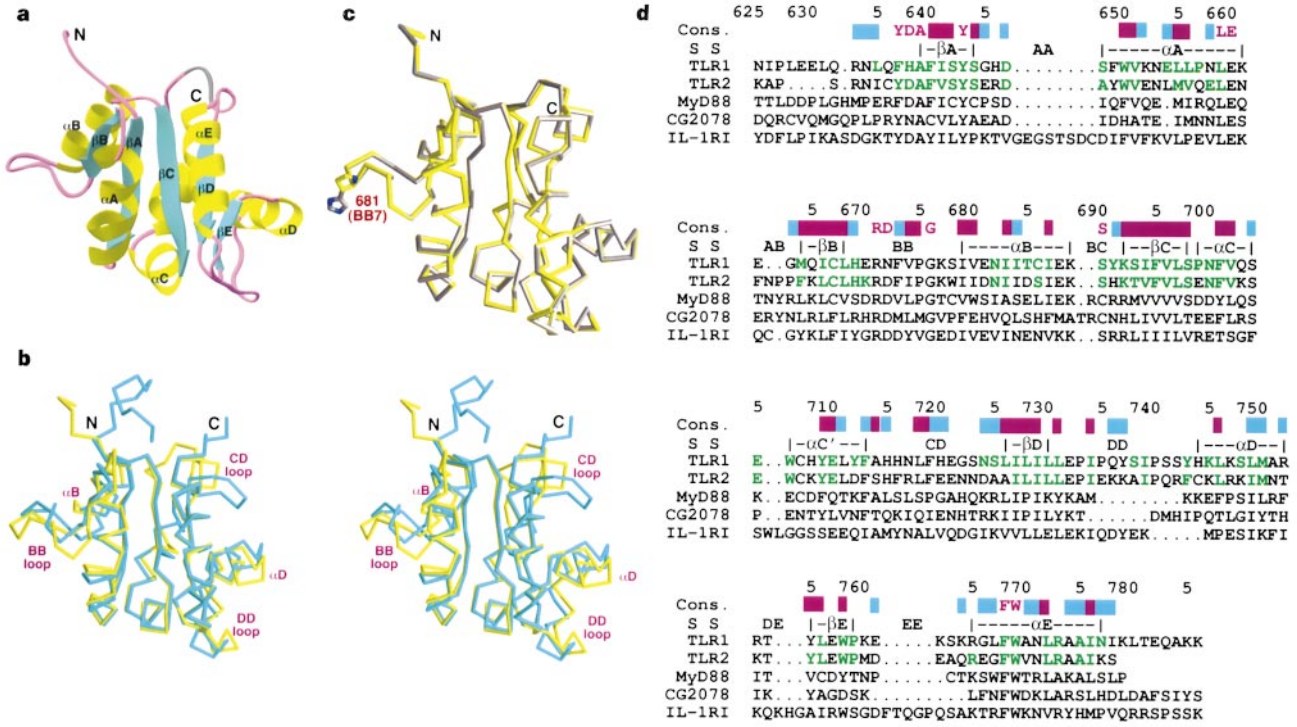

Figure 1 Structures of the TIR domain. **a**, Drawing of the structure of the TIR domain of human TLR2. Three missing residues, 723–725, are shown in grey. **b**, Superposition of the Cα traces of the structures of the TIR domain of human TLR1 (cyan) and TLR2 (yellow). Regions of large differences between the two structures are labelled. **c**, Superposition of the Cα traces of the structures of the TIR domain of human TLR2 wild type (yellow) and the P681H mutant (grey). The side chains of residue 681 are shown. **d**, Alignment of representative TIR domain sequences. The secondary structure elements (SS) are labelled. Amino-acid sequence conservation (Cons.) is indicated by the consensus residue name or a purple bar. Cyan bars indicate residues conserved in IL-1Rs or TLRs only. Residues in the hydrophobic core of the two structures (with less than 25% exposed surface area) are coloured in green. **a** produced with Ribbons[28], **b** and **c** with Grasp[29].

according to its position relative to the nearest strand or helix. For example, the residue immediately preceding strand βA can be numbered as βA-1.

The structures reveal that the core TIR domain starts from the conserved (F/Y)DA amino-acid motif and ends roughly eight residues carboxy-terminal to the conserved FW motif (Fig. 1d). The alanine residue of the (F/Y)DA motif is the first residue in strand βA (the βA1 residue). The amino and carboxy termini of this core TIR domain are located within 14 Å of each other, suggesting that the TIR domain may be considered as a cassette. Most of the conserved residues are located in the hydrophobic core of the structure. There are large insertions or deletions in several loop regions in different TIR domains. Consequently, the sizes of the core TIR domains vary considerably—between 135 and 160 residues among the sequences reported so far.

Although the TIR domains of TLR1 and TLR2 share 50% amino-acid sequence identity, there are large conformational differences between the two structures (for example, helices αB, αC′, and αD) (Fig. 1b). Noting that the sequence conservation among TIR domains is generally in the 20–30% range, as well as the variation in the sizes of the domains, our studies suggest that TIR domains may have a significant amount of sequence and structural diversity. This diversity may be crucial for the specificity in the signal transduction process, by ensuring the formation of the proper signalling complex among the many TLRs and IL-1Rs.

Three types of TIR domain interactions are possible for receptor signalling in animals. The first interface (which we call the R face) would mediate the oligomerization of receptor TIR domains, facilitated by the ligand-induced association of the extracellular domains of the receptors. The second interface (the A face, possibly equivalent to the R face in the receptor) would mediate the oligomerization of the TIR domains of the downstream adapter molecule (MyD88), which may be facilitated by death domain interactions in this molecule. It has been shown that MyD88 exists as dimers in solution[11]. The third interface (the S face) would mediate the association between the receptor and adapter TIR domains, and the formation of this TIR domain complex is critical for receptor signalling[7–11]. In *Drosophila*, the gene CG2078 has the same domain organization as MyD88 and may therefore be a functional homologue of MyD88, suggesting that the TIR domain signalling complex may be conserved between insects and mammals.

The interactions that take place at the R face are probably a main determinant of specificity in the receptor signalling process, in addition to those between the ligand and the receptor. This is supported by the observation that chimaeric receptor containing the extracellular domain of IL-1R type I (IL-1RI) and the intracellular domain of TLR1 cannot function in response to IL-1 (ref. 13), a possible explanation being that the TIR domains of the IL-1R accessory protein and TLR1 cannot form a proper complex. Therefore, it is likely that interactions at the R face may show a significant degree of diversity to allow for the specificity, consistent with the sequence and structural diversity that we have observed. Residues at this interface are probably not strictly conserved among the various receptor TIR domains.

In contrast, interactions at the S face should be primarily mediated by a highly conserved region among the TIR domains. Despite the identification of more than 20 TLRs and IL-1Rs in mammals, only one putative adapter molecule (MyD88) is currently known to contain a TIR domain[7–11]. Tollip has recently been identified as a receptor-proximal component of the IL-1RI pathway, but it does not contain a TIR domain[14]. In *Drosophila*, there are a

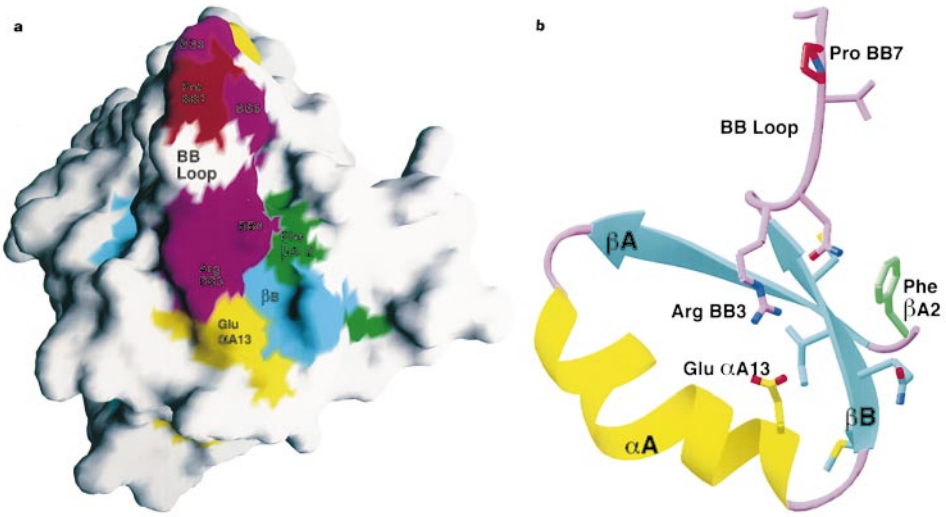

Figure 2 Structural analysis of the TIR domains. **a**, A large patch of conserved surface involving residues in the BB loop. Molecular surface of the TIR domain of TLR2 is shown. Conserved residues are highlighted in β-strands (cyan) in helices (yellow), in the BB loop (purple) and in other loops (green). The site of the Lps^d mutation (Pro BB7) is coloured in red. **b**, Drawing of the residues contributing to the conserved surface patch shown in **a**, in a similar orientation and colouring scheme. Also shown is the ion-pair between Arg BB3 and Glu αA13. **a** produced with Grasp[29] and **b** with Ribbons[28].

total of nine Toll homologues, but there is only one putative MyD88 homologue (CG2078). For this large number of receptors to signal through a common adapter molecule, the receptors must present a conserved surface area (S face) for coupling to the downstream adapter.

To identify the surface feature of the TIR domains that may be important for the recruitment of MyD88 (the S face), we analysed the molecular surface of the TIR domain in terms of amino-acid sequence conservation. This analysis reveals a large conserved surface patch (Fig. 2a), which mostly contains the BB loop, with additional contributions from helix αA, strand βB and the aromatic side chain of the (F/Y)DA motif (the βA-2 residue). The BB loop extends away for the rest of the TIR domain, forming a protrusion on the surface of the structure (Fig. 1a). This loop contains three highly conserved residues, Arg BB3, Asp BB4 and Gly BB8, in the RDx$\Phi_1\Phi_2$G motif (where Φ represents a hydrophobic residue, and x any residue). The side chains of both hydrophobic residues are exposed in the structure (Fig. 2a). The Arg BB3 residue has ion-pair interactions with the Asp BB4 residue (asparagine in TLR1 and TLR6 only) and the strictly conserved glutamate residue near the end of helix αA (Glu αA13) (Fig. 2b). The conformational difference for the BB loop in TLR2 (Fig. 1b) is probably due to the cacodylate modification of Cys βB4 during crystallization (see Methods), which is situated directly below the loop.

We performed functional studies to show that this conserved surface patch is crucial for signal transduction by the receptors. On the basis of the structural information, we mutated residues in this surface region and tested their functional effects using transfection assays with human TLR4 and *Drosophila* Toll[10,15]. These studies show that mutations at almost every position in this region lead to significantly reduced signalling activity of the receptors (Fig. 3a). Residues that were mutated include BB3, BB4, BB7 and BB8 in the BB loop, and residue αA13 (Fig. 3a). In addition, it has been reported that mutation of the BB3 residue in IL-1RI (R to A)[16] and the βA-2 residue of *Drosophila* Toll (F to I)[5] also blocked receptor signalling. The ion-pair between Arg BB3 and Glu αA13 seems to stabilize the conformation of the BB loop. Notably, the double mutant, BB3 R to E and αA13 E to R, could not rescue the signalling activity (Fig. 3a). It is likely that this ion-pair is involved in additional interactions in the signalling complex, or that the double mutant did not fully restore the ion-pair interactions.

The importance of this surface patch for receptor signalling is also emphasized by the fact that the Lps^d mutation[6] in murine TLR4, P712H, is at the Φ_2 position in the BB loop (residue BB7). To understand the structural basis for the elimination of receptor signalling caused by this mutation[6,7], we determined the crystal structure of the P681H mutant of the TLR2 TIR domain (Table 1). There are no significant structural differences between this mutant and the wild type (Fig. 1c). The mutation site is located at the tip of the BB loop, farthest from the rest of the TIR domain. The structures show that the proline residue does not have a special structural role. The lack of signalling by the Lps^d mutation is thus not due to disruption of the TIR domain structure itself, but rather to the disruption of a direct point of contact with other molecule(s), and specifically other TIR domains. Our observations are in contrast to those for the Fas death domain, where a naturally occurring mutation (V to N) eliminates signalling by destroying the native conformation of the domain[17]. The structural analysis is consistent with sequence and functional observations, as small hydrophobic residues (alanine, valine, isoleucine) are present at the BB7 position in several TIR domains (Fig. 1d). *Drosophila* Toll contains a valine residue at the BB7 position, and our studies showed that a V to P mutation has little effect on the function of the receptor (Fig. 3a). In contrast, a V to H mutation, equivalent to the Lps^d mutation of TLR4, as well as mutation to arginine or glutamate at the BB7 position, greatly reduced receptor function (Fig. 3a).

To understand further the molecular mechanism for the disruption of signalling by the Lps^d mutation and other changes of this conserved surface patch, we performed protein-binding assays between purified recombinant glutathione *S*-transferase (GST) fusion TIR domains and *in vitro* translated TIR domains. The binding assays show that there is a significant interaction between the TIR domains of MyD88 and TLR2, and also that the P681H

Table 1 Summary of crystal structure information

Structure	TLR1	TLR2	TLR2 (P681H)
X-ray source	CHESS A1	APS ComCAT	APS ComCAT
Maximum resolution (Å)	2.9	3.0	2.8
Cell parameters (*a*, *c*) (Å)	101.3, 137.9	121.2, 91.6	122.1, 92.1
R/free *R* factor* (%)	25.4/29.6	24.4/27.4	24.2/28.4

*$R = \Sigma_h |F_h^o - F_h^c| / \Sigma_h F_h^o$

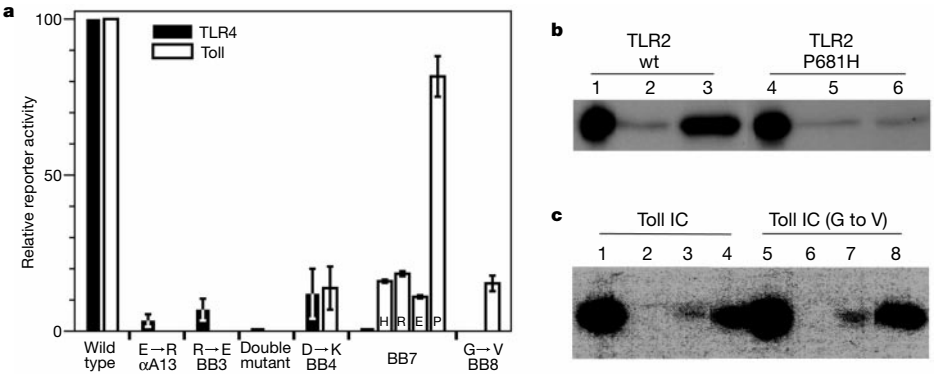

Figure 3 Functional studies of TIR domains. **a**, The relative signalling activity of mutants of human TLR4 (filled bars) and *Drosophila* Toll (open bars). At the BB7 position, the TLR4 mutant contained the P to H change (the Lps^{d} mutation), and the Toll mutant contains the V to H, R, E and P changes (as labelled). **b**, Protein-binding assays with MyD88 and TLR2 TIR domains, showing that the P681H mutation in TLR2 essentially abolished interactions with MyD88. Lanes 1 and 4, 10% of input ^{35}S-labelled protein (for expression level control); 2 and 5, GST only (control); 3 and 6, GST–MyD88. **c**, Protein-binding assays with *Drosophila* Toll[18], showing that the G–V mutation at the BB8 position does not interfere with receptor self-association. Lanes 1 and 5, 20% of input ^{35}S-labelled protein; 2 and 6, GST only (control); 3 and 7, GST–Toll IC; 4 and 8, GST–Pelle (K240R).

mutant of TLR2 almost completely abolished this interaction (Fig. 3b). At the same time, mutations in this surface patch do not seem to affect the oligomerization of the receptor (interactions at the R face), as shown by the binding assays with the G to V mutant at the BB8 position of *Drosophila* Toll (Fig. 3c). The experiment also shows that the previously documented interaction with the Pelle kinase was not affected by the mutation (Fig. 3c)[18]. Our biochemical data are supported by the observation that the intracellular domain of TLR4 containing the Lps^{d} mutation is a potent inhibitor of tumour-necrosis factor production in response to LPS stimulation as signalled by endogenous (full-length) TLR4 (ref. 19). Overall, the experimental data provide strong evidence that the R face is not disturbed by the Lps^{d} mutation. Both structural and functional studies therefore suggest that the conserved surface patch corresponds to the S face and that the Lps^{d} mutation abolishes receptor signalling by disrupting the recruitment of MyD88.

The backbone topology of the TIR domain is similar to that of the chemotaxis regulator CheY, as was proposed earlier[20], as well as many other proteins. The structural similarity between the TIR domain and CheY is however limited to the strands of the β-sheet (see Supplementary Information). In addition, TIR domains do not contain a cation-binding site equivalent to that in CheY (ref. 21), and therefore have a different mechanism of action from the response regulators. Nonetheless, it is interesting to note that a domain of similar architecture is used for signal transduction in response to exogenous stimulus in bacteria and eukaryotes.

We performed gel-filtration and dynamic light-scattering experiments to characterize the oligomerization state of isolated TIR domains in solution. These studies indicate that the inherent affinity for self-association of the TIR domains is rather low (dissociation constant (K_d) in the millimolar range; data not shown). At high concentrations, dimers and tetramers of TIR domains are observed in solution. This low affinity is consistent with the observation that signal transduction through TIR domains requires receptor oligomerization, induced either by ligand binding or by overexpression[7–11]. It is likely that avidity may be important in the assembly of the TIR domain signalling complex. Our structural and functional information provide a molecular basis for understanding the mechanism and complexity of signal transduction by the TIR domains. □

Methods

Protein production and crystallization

Details on the expression, purification and crystallization of the TIR domains of human TLR1 and TLR2 will be presented elsewhere. Briefly, the TIR domain of human TLR1 (residues 625–786, about 20 residues from the transmembrane region) was overexpressed in *Escherichia coli* and purified with nickel-agarose, cation exchange and gel-filtration chromatography. We purified the TIR domain of TLR2 (residues 626–784; about 16 residues from the transmembrane region) with cation exchange and gel-filtration chromatography. The P681H mutant of this domain was produced with the QuickChange mutagenesis kit (Stratagene) and sequenced to confirm the presence of the mutation. We obtained crystals of the TIR domain of TLR1 at 21 °C by the hanging-drop vapour-diffusion method. The reservoir solution contained 100 mM Tris (pH 8.0), 1.2 M NaH_2PO_4/K_2HPO_4, 5 mM dithiothreitol (DTT) and 20% glycerol. The crystals belong to space group $P6_422$. The TIR domain of TLR2 was crystallized at 4 °C. The reservoir solution contained 100 mM cacodylate (pH 6.8), 10% PEG 8,000, 20% (v/v) DMSO, 200 mM $MgCl_2$ and 5 mM DTT. The crystals belong to space group $P6_222$.

Structure determination

We collected X-ray diffraction data using rotating anode and synchrotron radiation sources (32-ID beamline (ComCAT) at APS, X4A beamline at NSLS and A-1 beamline at CHESS). The diffraction images were processed and scaled with the HKL package[22]. For TLR1, phases were obtained from the selenomethionyl multiwavelength anomalous diffraction (MAD) method[23] and the multiple isomorphous replacement (MIR) method[24]. The atomic model was built with the program O (ref. 25). We carried out the structure refinement with the program CNS[26]. There is a disulphide bond between Cys 707 and its twofold symmetry mate, which was confirmed by non-reducing SDS–PAGE and MALDI-TOF analysis on the crystals. A comparison with the structure of the TIR domain of TLR2 shows that the disulphide bond did not introduce significant conformational changes in the TIR domain of TLR1.

We determined the initial structure of the TIR domain of TLR2 by the combined molecular replacement protocol as implemented in the Replace package[27], using the structure of TIR domain of TLR1 as the model. The cysteine side chains had been modified by the cacodylate buffer, and the anomalous diffraction contained contributions from both Se and As atoms. The acentric reflections were phased with the anomalous diffraction data, and the centric reflections were phased with the molecular replacement solution. See Supplementary Information for more details on the structure determination.

There is only one molecule of the TIR domain in the asymmetric unit for crystals of both TLR1 and TLR2. This gives rise to a solvent content of about 80% and a unit cell volume to mass ratio of 5.5 Å^3 per dalton for these crystals.

Functional studies with human TLR4 and *Drosophila* Toll

A truncated version of human TLR4, containing residues 558–825 and lacking the leucine-rich-repeat domain, was used for the mammalian functional studies as it has a higher constitutive activity. The mutants were made by site-directed polymerase chain reaction (PCR) mutagenesis and cloned into the pFLAG CMV1 vector. The receptor activity was measured by its ability to activate an NF-κB-dependent luciferase reporter after transient transfections of 2 μg of DNA into 293T cells[10]. The T110b mutant of Toll, which contains a C to Y mutation in its extracellular domain[5], was used for the functional studies in *Drosophila* cells as it has a higher constitutive activity[15]. The mutants were made by site-directed mutagenesis with the QuickChange kit (Stratagene). We assayed signalling activity by co-transfection of 2 μg of Toll and 0.4 μg of dorsal expression vectors and a dorsal-dependent chloramphenicol acetyl transferase (CAT) reporter into *Drosophila* Schneider cells[15]. In both systems, all mutants were sequenced to confirm the presence of the respective mutations, and the assays were repeated several times to ensure reproducibility. Equivalent expression levels of the wild-type and mutant proteins were verified by western blotting.

Protein binding assays

The TIR domain of MyD88 was purified as a GST fusion protein, immobilized with

glutathione-agarose and incubated with [^{35}S]methionine-labelled wild type and P681H mutant of the TIR domain of TLR2 that were obtained by *in vitro* translation (Promega TNT system). For *Drosophila* Toll, the purified intracellular domain (GST–Toll IC) and GST–Pelle (K240R mutant) were incubated with [^{35}S]methionine-labelled intracellular domains of wild-type Toll and the G to V mutant at the BB8 position[18]. After washing, the bound proteins were eluted and separated by SDS–PAGE. Gels were fixed and exposed to X-ray film.

Received 12 July; accepted 11 September 2000.

1. Hoffmann, J. A., Kafatos, F. C., Janeway, C. A. Jr & Ezekowitz, R. A. B. Phylogenetic perspectives in innate immunity. *Science* **284,** 1313–1318 (1999).
2. Kopp, E. B. & Medzhitov, R. The Toll-receptor family and control of innate immunity. *Curr. Opin. Immunol.* **11,** 13–18 (1999).
3. Anderson, K. V. Toll signaling pathways in the innate immune response. *Curr. Opin. Immunol.* **12,** 13–19 (2000).
4. Gay, N. J. & Keith, F. J. *Drosophila* Toll and IL-1 receptor. *Nature* **351,** 355–356 (1991).
5. Schneider, D. S., Hudson, K. L., Lin, T.-Y. & Anderson, K. V. Dominant and recessive mutations define functional domains of Toll, a transmembrane protein required for dorsal-ventral polarity in the Drosophila embryo. *Genes Dev.* **5,** 797–807 (1991).
6. Poltorak, A. *et al.* Defective LPS signaling in C3H/HeJ and C57BL/10ScCr mice: mutations in Tlr4 gene. *Science* **282,** 2085–2088 (1998).
7. Underhill, D. M. *et al.* The Toll-like receptor 2 is recruited to macrophage phagosomes and discriminates between pathogens. *Nature* **401,** 811–815 (1999).
8. Muzio, M., Ji, J., Feng, P. & Dixit, V. M. IRAK (Pelle) family member IRAK-2 and MyD88 as proximal mediators of IL-1 signaling. *Science* **278,** 1612–1615 (1997).
9. Wesche, H., Henzel, W. J., Shilinglaw, W., Li, S. & Cao, Z. MyD88, an adapter that recruits IRAK to the IL-1 receptor complex. *Immunity* **7,** 837–847 (1997).
10. Medzhitov, R. *et al.* MyD88 is an adaptor protein in the hToll/IL-1 receptor family signaling pathways. *Mol. Cell* **2,** 253–258 (1998).
11. Burns, K. *et al.* MyD88, an adapter protein involved in interleukin-1 signaling. *J. Biol. Chem.* **273,** 12203–12209 (1998).
12. Eck, M. J., Schoelson, S. E. & Harrison, S. C. Recognition of a high-affinity phosphotyrosyl peptide by the Src homology-2 domain of p56lck. *Nature* **362,** 87–91 (1993).
13. Mitcham, J. L. *et al.* T1/ST2 signaling establishes it as a member of an expanding interleukin-1 receptor family. *J. Biol. Chem.* **271,** 5777–5783 (1996).
14. Burns, K. *et al.* Tollip, a new component of the IL-1RI pathway, links IRAK to the IL-1 receptor. *Nature Cell Biol.* **2,** 346–351 (2000).
15. Norris, J. L. & Manley, J. L. Selective nuclear transport of the *Drosophila* morphogen dorsal can be established by a signaling pathway involving the transmembrane protein Toll and protein kinase A. *Genes Dev.* **6,** 1654–1667 (1992).
16. Slack, J. L. *et al.* Identification of two major sites in the type I interleukin-1 receptor cytoplasmic region responsible for coupling to pro-inflammatory signaling pathways. *J. Biol. Chem.* **275,** 4670–4678 (2000).
17. Huang, B., Eberstadt, M., Olejniczak, E. T., Meadows, R. P. & Fesik, S. W. NMR structure and mutagenesis of the Fas (APO-1/CD95) death domain. *Nature* **384,** 638–641 (1996).
18. Shen, B. & Manley, J. L. Phosphorylation modulates direct interactions between the Toll receptor, Pelle kinase and Tube. *Development* **125,** 4719–4728 (1998).
19. Du, X., Poltorak, A., Silva, M. & Beutler, B. Analysis of Tlr4-mediated LPS signal transduction in macrophages by mutational modification of the receptor. *Blood Cells Mol. Dis.* **25,** 328–338 (1999).
20. Rock, F. L., Hardiman, G., Timans, J. C., Kastelein, R. A. & Bazan, J. F. A family of human receptors structurally related to *Drosophila* Toll. *Proc. Natl Acad. Sci. USA* **95,** 588–593 (1998).
21. Stock, J. B., Stock, A. M. & Mottonen, J. M. Signal transduction in bacteria. *Nature* **344,** 395–400 (1990).
22. Otwinowski, Z. & Minor, W. processing of X-ray diffraction data collected in oscillation mode. *Methods Enzymol.* **276,** 307–326 (1997).
23. Hendrickson, W. A. Determination of macromolecular structures from anomalous diffraction of synchrotron radiation. *Science* **254,** 51–58 (1991).
24. Furey, W. & Swaminathan, S. PHASES-95: A program package for processing and analyzing diffraction data from macromolecules. *Methods Enzymol.* **277,** 590–620 (1997).
25. Jones, T. A., Zou, J. Y., Cowan, S. W. & Kjeldgaard, M. Improved methods for building protein models in electron density maps and the location of errors in these models. *Acta Crystallogr. A* **47,** 110–119 (1991).
26. Brunger, A. *et al.* Crystallography & NMR System: A new software suite for macromolecular structure determination. *Acta Crystallogr. D* **54,** 905–921 (1998).
27. Tong, L. Combined molecular replacement. *Acta Crystallogr. A* **52,** 905–921 (1998).
28. Carson, M. Ribbon models of macromolecules. *J. Mol. Graph.* **5,** 103–106 (1987).
29. Nicholls, A., Sharp, K. A. & Honig, B. Protein folding and association: insights from the interfacial and thermodynamic properties of hydrocarbons. *Proteins Struct. Funct. Genet.* **11,** 281–296 (1991).

Supplementary information is available on *Nature*'s World-Wide Web site (http://www.nature.com) or as paper copy from the London editorial office of *Nature*. The atomic coordinates have been deposited in the protein Data Bank under accession numbers IFYU, IFYW, IFYX.

Acknowledgements

We thank K. D'Amico and S. Wasserman for setting up the beamline at the Advanced Photon Source (APS) (supported by the US Department of Energy), R. Abramowitz and C. Ogata for setting up the beamline at the National Synchrotron Light Source (NSLS), and the MacCHESS staff for setting up the beamline at CHESS. We thank G. Bhargava, L. Duan and G. Xu for technical help; R. Khayat, G. Jogl, and Z. Yang for help with data collection at the synchrotron sources; H. Wu and W. Hendrickson for discussions; and Columbia University (L.T.) and an NIH grant (J.L.M.) for financial support.

Correspondence and requests for materials should be addressed to L.T. (e-mail: tong@como.bio.columbia.edu).

Structural basis for the activation of 20S proteasomes by 11S regulators

Frank G. Whitby*†, Eugene I. Masters*†, Larissa Kramer*, J. Randolph Knowlton*, Yi Yao‡, Ching C. Wang‡ & Christopher P. Hill*

* *Biochemistry Department, University of Utah, 50 N Medical Drive, Salt Lake City, Utah 84132, USA*
‡ *Department of Pharmaceutical Chemistry, University of California, San Francisco, California 94143-0446, USA*
† *These authors contributed euqally to this work*

Most of the non-lysosomal proteolysis that occurs in eukaryotic cells is performed by a nonspecific and abundant barrel-shaped complex called the 20S proteasome[1]. Substrates access the active sites, which are sequestered in an internal chamber, by traversing a narrow opening[2] (α-annulus) that is blocked in the unliganded 20S proteasome by amino-terminal sequences of α-subunits[3]. Peptide products probably exit the 20S proteasome through the same opening. 11S regulators (also called PA26 (ref. 4), PA28 (ref. 5) and REG[6,7]) are heptamers[4,8,9] that stimulate 20S proteasome peptidase activity *in vitro* and may facilitate product release *in vivo*. Here we report the co-crystal structure of yeast 20S proteasome with the 11S regulator from *Trypanosoma brucei*[4] (PA26). PA26 carboxy-terminal tails provide binding affinity by inserting into pockets on the 20S proteasome, and PA26 activation loops induce conformational changes in α-subunits that open the gate separating the proteasome interior from the intracellular environment. The reduction in processivity expected for an open conformation of the exit gate may explain the role of 11S regulators in the production of ligands for major histocompatibility complex class I molecules[10,11].

After unsuccessful efforts to crystallize a complex of an 11S regulator and a 20S proteasome from the same species, we attempted to crystallize heterologous complexes. This approach was justified by the ability of 11S regulators to activate 20S proteasomes from widely divergent species. For example, trypanosome PA26 activates 20S proteasome from rat[4], and human REGα activates 20S proteasome from yeast (M. Rechsteiner, personal communication). We therefore used the fluorogenic substrate suc-LLVY-MCA[4] to show that recombinant PA26 stimulates the peptidase activity of yeast 20S proteasome by up to eightfold (data not shown).

We co-crystallized trypanosome PA26 and yeast 20S proteasome, and determined the structure at 3.2 Å resolution using the known structure of yeast 20S proteasome[3] as a molecular replacement search model (Fig. 1a). The asymmetric unit contains a complex of one 20S proteasome and two PA26 heptamers that has a relative molecular mass (M_r) of 1.1 million, a length of 290 Å and a maximum diameter of 120 Å (Fig. 1b). This structure resembles electron microscopy images of mammalian 11S regulator/20S proteasome complexes[12].

Despite sharing only 14% sequence identity, the structure of PA26 resembles that of the human 11S regulator, REGα[8]. The monomer, which comprises four long helices, packs into a heptamer that has overall dimensions of 90 Å in diameter and 70 Å in length (Fig. 2). Helices 2, 3 and 4, and the loop between helices 2 and 3 are quite similar in PA26 and REGα with r.m.s. deviation of 1.8 Å and maximum displacement of 3.6 Å for overlap on all 924 pairs of Cα atoms. Helix 1 occupies the same volume in PA26 and REGα, although it is not clear how these residues should be aligned, in part because Fourier maps are more poorly defined in this section. The heptamer surrounds a central pore of 33 Å in diameter at the proteasome-binding end and 24 Å in diameter at the distal end. The loop between helices 2 and 3 is primarily responsible for